BATCH: jp5b119 USER: mly69 DIV: @xyv04/data1/CLS_pj/GRP_jp/JOB_i18/DIV_jp0573341 DATE: March 23, 2006

Molecular Depth Profiling with Cluster Ion Beams

Juan Cheng,[†] Andreas Wucher,[‡] and Nicholas Winograd*[,†]

Chemistry Department, Pennsylvania State University, 104 Chemistry Building, University Park, Pennsylvania 16802, and Physics Department, University of Duisburg-Essen, 47048 Duisburg, Germany

Received: December 15, 2005; In Final Form: March 3, 2006

Peptide-doped trehalose thin films have been characterized by bombardment with energetic cluster ion beams of C_{60}^+ and Au_x^+ ($x = 1, 2, 3$). The aim of these studies is to acquire information about the molecular sputtering process of the peptide and trehalose by measurement of secondary ion mass spectra during erosion. This system is important since uniform thin films of ~300 nm thickness can be reproducibly prepared on a Si substrate, allowing detailed characterization of the resulting depth profile with different projectiles. The basic form of the molecular ion intensity as a function of ion dose is described by a simple analytical model. The model includes parameters such as the molecular sputtering yield, the damage cross section of the trehalose or the peptide, and the thickness of a surface layer altered by the projectile. The results show that favorable conditions for successful molecular depth profiling are achieved when the total sputtering yield is high and the altered layer thickness is low. Successful molecular depth profiles are achieved with all of the cluster projectiles, although the degree of chemical damage accumulation was slightly lower with C_{60}. With C_{60} bombardment, the altered layer thickness of about 20 nm and the damage cross section of about 5 nm^2 are physically consistent with predictions of molecular dynamics calculations available for similar chemical systems. In general, the model presented should provide guidance in optimizing experimental parameters for maximizing the information content of molecular depth profiling experiments with complex molecular thin film substrates.

1. Introduction

It has recently been shown that many types of organic thin films may be characterized in depth by erosion with energetic cluster ion beams followed by analysis with secondary ion mass spectrometry (SIMS).[1−6] The removal of a sizable amount of material from such structures without destroying molecular information is quite unusual since the traditional atomic projectiles generally leave the surface heavily damaged. As a consequence of this observation, three-dimensional molecule-specific imaging is being investigated with use of focused ion beam sources to achieve depth information in addition to lateral information.[7]

There is a growing list of examples where molecular depth profiling is being employed. With 8 keV SF_5^+ bombardment, a variety of polymers have been examined from characteristic molecular fragments.[5,8] It has also been possible to retain the molecular ion signal of small drug molecules doped into a polymer such as polylactic acid.[9] In this case, apparently the SF_5^+ projectile unzips the polymer backbone, allowing the embedded molecule to escape. In addition to SF_5^+ sources, metal cluster ion sources such as Au_3 [10] or Bi_3 [11] have become commercially available and are being developed for molecular depth profiling. Buckminsterfullerene (C_{60}) ion beams also demonstrate the unique ability to interact with organic surfaces without accumulating large amounts of damage and are showing great promise for these types of experiments.[2,12]

To investigate the fundamental aspects of the interaction of energetic cluster ion beams with organic materials, we have recently developed a model platform consisting of a uniform glassy film of trehalose.[2] This simple naturally occurring sugar formed by a 1,1 linkage of two D-glucose molecules is known to protect anhydrobiosis (life without water) in harsh dehydration environments[13−15] and has been utilized to enhance the stability of biomaterials, particularly peptides and proteins.[16,17] In this previous study, small peptides were doped at the 1% level into a film of trehalose of about 350 nm, spin-cast onto a Si wafer, and bombarded with 20 keV C_{60}^+. Because of the stability and uniformity of the films, it was feasible to characterize the sputtering yield of the trehalose and peptide molecules, and to examine issues such as depth resolution, topography formation, and damage accumulation. Our results showed that there were nearly 300 trehalose molecule equivalents removed for each C_{60}^+ impact. The molecular ion of each of the peptide molecules could be observed during removal of the entire film, using peptides with molecular weights ranging from 362 to 498. Moreover, the measured width at the trehalose/Si interface was on the order of 10 nm, indicating only a small amount of interlayer mixing during the bombardment. In general, the results support the notion that molecular depth profiling is feasible with cluster ion beams since the removal rate of material exceeds the rate of chemical damage created by the bombardment event.

At this stage of development, a more quantitative understanding of the factors that lead to successful depth profiling experiments would be useful for extending the applications of this methodology. Arguably, the best understanding of the sputtering of inorganic materials comes from molecular dynamics computer simulations where the yields, energy distributions, and angle distributions of emitted species can be compared with experiment.[18] These calculations on Ag[19,20] and on graphite,[21] for example, show that crater formation and the associated mesoscale motion is the essential feature of the enhanced yield associated with cluster bombardment. The calculations for

* Address correspondence to this author. E-mail: nxw@psu.edu.
[†] Pennsylvania State University.
[‡] University of Duisburg-Essen.

10.1021/jp0573341 CCC: $33.50
Published on Web 00/00/0000 PAGE EST: 7.2

projectiles of equivalent kinetic energies also suggest that ion beam induced topography is minimized and that interface mixing is virtually eliminated when compared to atomic bombardment.[22−24] These calculations are considerably more involved when modeling molecular systems, however. Considering that potential energy functions must include some information about bond breaking and that up to 2 million atoms are needed to contain the sputtering event, it is clear that the problem is challenging. Presently, calculations are underway with benzene[25] and ice[26] as models, but applications to molecular depth profiling are still in the future.

As a compliment to the MD approach, here we present a simple analytical model to embody the important variables that affect the shape of molecular depth profiles. This model is based on ideas presented in the 1990s by Gillen and Williams,[27] and appears particularly relevant now due to the quality of the experimental molecular depth profiles emerging from the trehalose system. In this paper, we extend the experimental approach described earlier[2] by utilizing peptides up to a molecular weight of 830, and present an improved method for characterizing the shape of the crater using atomic force microscopy (AFM). With these data and the simple model, it is possible to predict semiquantitatively the form of the depth profile as a function of the incident ion fluence. The results show that the key parameters in obtaining a successful molecular depth profile are the total removal rate of material relative to the damage depth created by the incident beam and the intrinsic damage cross section of the target molecule. For C_{60}^+ bombardment at 20 keV, the total yield of trehalose ranges from 200 to 250 molecule equivalents removed per projectile impact, depending upon the dopant, and the altered layer thickness is about 20 nm. Depth profiles created with metal cluster ions such as Au_3 fit the model less satisfactorily due to the implantation of Au atoms. Finally, using the parameters in the model, we suggest scenarios most likely to further improve the prospects for successful molecular depth profiling.

2. Experimental Section

2.1. Materials and Film Preparation. A detailed description of the preparation of the trehalose films has been described previously.[2] The peptides Gly-Gly-Tyr-Arg (GGYR) and Lys-Arg-Thr-Leu-Arg-Arg (KRTLRR) were obtained from Sigma-Aldrich (St. Louis, MO). To prepare a film, peptides were dissolved in water at concentrations of 10 mM and then mixed with the same volume of 1 M aqueous trehalose solution. The mixture was then spin-cast onto a pre-sliced 5 mm × 5 mm Si wafer (Ted Pella Inc., Redding, CA) spinning at a speed of about 3200 rpm. A uniformly colored film with a glassy appearance is normally obtained.

2.2. AFM and Yield Measurements. The amount of material removed during cluster bombardment is determined with an AFM (Nanopics 2100, KLA-Tencor, San Jose, CA) rather than the previously reported profilometer tracing. This method provides a more accurate representation of the volume of the resulting crater, which results in more reliable yield measurements. The AFM has a maximum field of view of 800 μm × 800 μm with contact mode, allowing various sized craters to be characterized within a single image. By calculating the volume of the crater, and accounting for the different sputtering rates of Si and of trehalose,[28] the number of trehalose molecules removed per incident projectile is determined, assuming the density of the film is equal to the density of trehalose (1.54 g/cm^3). The AFM was also employed to detect the presence of any topography that might build up during the course of film erosion by measuring the root-mean-square value of the surface. For these measurements, an area of 20 μm^2 of the irradiated surface was compared to the unirradiated portion of the film. Height fluctuations of about 1 nm could easily be detected with this equipment.

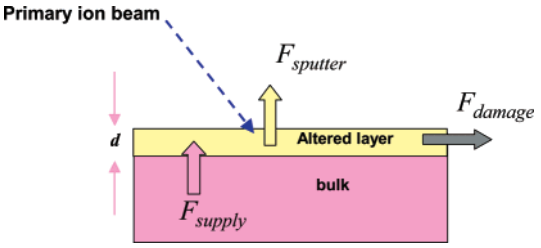

Figure 1. Schematic diagram of the erosion model. The variable F represents the indicated flux of intact molecules in to and out of the altered layer of thickness d.

2.3. Instrumentation. Depth profiles and TOF-SIMS spectra were recorded with previously described instrumentation.[2,29] Spectra were recorded with use of 50 ns pulses for bombardment, followed by delayed extraction of secondary ions with a delay of 100 ns. This procedure yielded a mass resolution of about 2000 above m/z 200. For depth profiling, a crater was created of a size on the order of 400 μm by 400 μm, and the spectra were taken from a zoomed region of one-quarter area size within the center of the crater with a total fluence of less than 10^{10} ions/cm^2. The C_{60} primary ion source, obtained from Ionoptika Ltd. (Southhampton, UK), was directed to the target at an angle of 40° relative to the surface normal. Details of the design of this source have been published.[30] The nominal kinetic energy of the C_{60}^+ Beam was chosen as 20 keV with a DC beam current of about 0.1 nA and a probe size typically about 20 μm in diameter. Contribution of ions other than C_{60}^+, for example C_{60}^{2+}, was minimized to less than 20% by keeping the electron impact ionization energy in the source below 40 eV. The Au cluster ion source was also obtained from Ionoptika Ltd, and was equipped with a Wien filter for selecting Au^+, Au_2^+, or Au_3^+ projectiles. A kinetic energy of 25 keV was employed for each of these species with DC beam currents of 1.6, 0.2, and 0.16 nA, respectively. The probe size from this liquid metal ion source was about 200 nm.

3. Results and Discussion

The goal of this work is to acquire a better understanding of the details of the shape of the molecular depth profile obtained under cluster bombardment. To examine some of the factors that are important, we first present a simple model of the erosion process that includes parameters which may be tested experimentally. The predictions of this model are then compared to experimentally determined profiles for films of trehalose and peptide-doped trehalose films interrogated with the entire suite of available projectiles.

3.1. Erosion Model. *3.1.1. Single-Component Molecular Thin Film.* We begin with a simple model, as shown in Figure 1, describing the ion bombardment induced erosion of a molecular thin film. The treatment is based on the following assumptions:

(i) There is a dimensionless concentration, c, of intact molecules that changes with ion fluence due to sputter removal and ion-induced damage in an altered layer of thickness d beneath the surface. The surface concentration of these molecules is c_s; and the bulk concentration, found at depths larger than d, is c_b.

(ii) The surface is eroded with a constant total sputtering yield, Y^{tot}, that is given in molecular equivalents removed per projectile impact.

(iii) Each projectile impact creates chemical damage by destroying all molecules within the damage cross section, σ_D, across the entire altered layer.

(iv) The molecular ion signal, S, of the investigated species is proportional to the corresponding partial sputter yield, which, in turn, is proportional to the corresponding value of c_s.

With the above assumptions, this model describes the primary ion fluence dependence of the surface concentration of intact molecules, c_s, as

$$\frac{dc_s}{df} = \frac{Y^{tot}c_b}{nd} - \frac{Y^{tot}c_s}{nd} - \sigma_D c_s \quad (1)$$

where f is the primary ion fluence, and the parameter n denotes the density of molecules in the sample. The first term on the right side describes the supply of undamaged material from the bulk to the modified layer, which is induced by the erosion of the sample. The second term denotes the loss of molecules from the surface due to sputtering, while the third term describes the additional loss of intact molecules generated by ion bombardment-induced damage.

According to assumption iv, the intensity S of the molecular signal is proportional to c_s, and the solution of eq 1 can be given as

$$S(f) = S_{ss} + (S_0 - S_{ss}) \exp\left[-\left(\frac{Y^{tot}}{nd} + \sigma_D\right)f\right] \quad (2)$$

where S_0 is the signal intensity at zero fluence and S_{ss} is the signal intensity at steady state. The quantity in parentheses appearing in the exponent on the right side of eq 2 represents the exponential slope, which can be extracted from the experimental data and is referred to as the effective "disappearance cross section", σ_{eff},

$$\sigma_{eff} = \frac{Y^{tot}}{nd} + \sigma_D \quad (3)$$

Note that this value represents an upper limit for σ_D.

Under steady-state conditions, where $dc_s/df = 0$, eq 1 predicts

$$c_s = c_b \frac{Y^{tot}}{Y^{tot} + nd\sigma_D} \quad (4)$$

Assuming that the sample is homogeneous at the beginning of the depth profile experiment, c_s/c_b is equal to S_{ss}/S_0. The value of S_{ss} is therefore determined by

$$S_{ss} = S_0 \frac{Y^{tot}}{Y^{tot} + nd\sigma_D} \quad (5)$$

In eq 5, the relative values of Y^{tot} and $nd\sigma_D$ allow estimation of the influence of damage accumulation with respect to sputter removal of molecules from the surface. If $Y^{tot} \gg nd\sigma_D$, minimal chemical damage is expected, and $S_{steadystate}$ should be close to the value obtained under low dose bombardment conditions. As a consequence, molecular information is maximized when the altered layer thickness is small and the total sputtering yield is large.

3.1.2. Multicomponent Molecular Thin Film. This model may, in principle, be extended to include multicomponent molecular thin films. Here, we are interested in the behavior of dopant (peptide) molecules in the host matrix (trehalose) at about the 1% concentration level. For this situation, the change in the dimensionless concentration of the analyte, c^a, with incident ion fluence is described by

$$\frac{dc_s{}^a}{df} = \frac{Y^{tot}c_b{}^a}{nd} - \frac{Y^a}{nd} - \sigma_D c_s{}^a \quad (6)$$

where the superscript "a" refers to any analyte molecule, matrix or dopant, present in the sample. In analogy to eq 1, the first term on the right side of eq 6 describes the supply of undamaged analyte molecules from the bulk to the modified layer, which is induced by the erosion of the sample. Note that this supply term is controlled not only by the analyte concentration in the bulk, but also by the total sputtering yield of the system, including both matrix and dopant species. The second term denotes the loss of analyte molecules from the surface due to sputtering, with Y^a being defined as the partial sputtering yield of analyte molecules.

The evaluation of Y^a requires special consideration. In our experiments, the dopant is present at the 1% level, so it exerts only a small effect on Y^{tot}. According to assumption iv, Y^a should be proportional to the analyte surface concentration c_s^a in the modified layer as

$$Y^a = Y_0{}^a c_s^a \quad (7)$$

where $Y_0{}^a$ is a proportionality constant. Although this approximation is oversimplified, it still allows a qualitative description of the expected trends. For matrix molecules, $Y_0{}^a$ is equal to the total sputter yield Y^{tot}. For dopant molecules, on the other hand, the value of $Y_0{}^a$ may depend on a number of factors, including concentration-dependent interactions between dopant and matrix molecules, physical changes in the altered layer during erosion, and changes in the sputtering characteristics for peptide films of high concentration. For these species, the validity of eq 7 is therefore restricted to conditions where $c_s{}^a \ll 1$, and the value of $Y_0{}^a$ determined under these conditions is unlikely to reflect the actual sputtering yield of a pure peptide film.

Solution of eq 6 yields an equation of the same form as that reported in eq 2 as

$$S(f) = S_{ss}{}^a + (S_0{}^a - S_{ss}{}^a) \exp\left[-\left(\frac{Y_0{}^a}{nd} + \sigma_D\right)f\right] \quad (8)$$

and

$$\sigma_{eff}{}^a = \frac{Y_0{}^a}{nd} + \sigma_D \quad (9)$$

In steady state, a very similar relation to that shown in eq 5 results for the peptide-doped films as:

$$S_{ss}{}^a = S_0{}^a \frac{Y^{tot}}{Y_0{}^a + nd\sigma_D} \quad (10)$$

The magnitude of the analyte molecular ion signal depends on very similar factors as those discussed for the pure matrix. The relation between Y^{tot} and $Y_0{}^a$, however, introduces interesting predictions. If $Y_0{}^a = Y^{tot}$, then the analyte and the matrix will be removed at the same rate. Note again that this is naturally the case if the analyte is the matrix itself. If $Y_0{}^a > Y^{tot}$, however, then preferential sputtering of analyte molecules would cause the analyte concentration to decrease with incident ion fluence. Hence, it is possible that the signal decrease with fluence observed for any analyte except the matrix may result not only

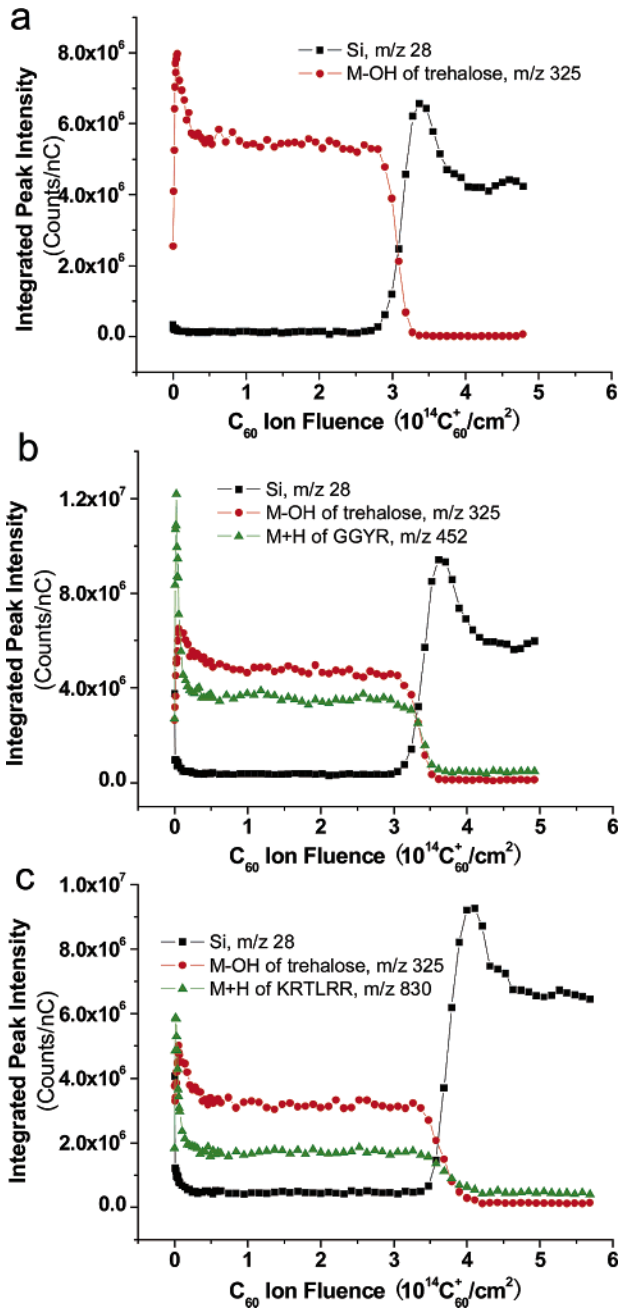

Figure 2. Secondary ion signal intensities versus accumulated C_{60}^+ ion fluence during depth profiling of (a) a pure trehalose film (270 nm), (b) a trehalose film doped with 1% GGYR (263 nm), and (c) a trehalose film doped with 1% KRTLRR (273 nm).

from chemical damage associated with the $nd\sigma_D$ term, but also from preferential sputtering due to the relative values of Y^{tot} and $Y_0{}^a$.

3.2. Depth Profiles of Pure Trehalose Films Bombarded by C_{60}^+. The shape of a typical trehalose molecular depth profile is illustrated in Figure 2a for a pure 270 nm trehalose film on Si bombarded by C_{60}^+. There are fluctuations in intensity up to a fluence of approximately 2×10^{13} ions/cm^2. This signal then remains constant until the entire film is removed and the Si substrate is reached. We assume that the initial increase in molecular ion signal arises in part from a change in the electronic properties of the surface due to perturbations associated with the incident ion beam, or to removal of surface contaminants, which ultimately affects the ionization probability of the molecules. This disruption zone is reflected in similar variations of the intensity of ions at *m/z* 15, 18, 19, and other fragment

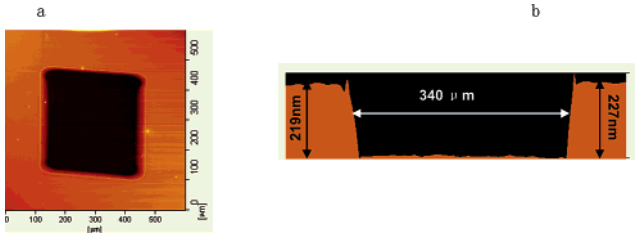

Figure 3. AFM images of a typical C_{60}^+ depth profile crater and the respective cross section of a trehalose film. The field of view is 400 μm $\times$ 400 μm in part a. The dimension and depth of the crater were measured as shown in the cross section image (b).

ions as reported earlier.[2] The subsequent decline of the signal before steady state is then attributed to the buildup of chemical damage. Eventually, the disappearance rate induced by removal of intact analyte molecules from the altered layer and the supply rate induced by the surface erosion reach equilibrium, and a steady state is achieved.

On the basis of crater volume, there are 245 $\pm$ 7 trehalose molecule equivalents removed per incident C_{60}^+. This number is somewhat lower than the value reported earlier,[2] the discrepancy being primarily due to the more accurate capability of the AFM than the previously employed profilometer to determine crater volume. The yield may also vary depending upon the precise film preparation protocol and includes such variables as laboratory temperature and humidity. A cross section of a crater is shown in Figure 3. To be sure that the erosion is being performed in a uniform fashion without the buildup of topography, the AFM was employed to examine the roughness of the sugar film on the virgin and the irradiated surface. As can be seen from the images in Figure 4, the bombardment process does not alter the topography in any measurable way, at least to the subnanometer resolution of the AFM. This result supports the qualitative observations made earlier with the profilometer. Finally, we estimate the interface width at the trehalose−Si interface to be about 7 nm. Details of this analysis have also been reported previously.[2]

With the above experimental data, it is possible to compare the depth profile to the predictions of the model developed in section 3.1and to extract the relevant parameters. The first step is to determine the starting signal S_0 and the effective disappearance cross section σ_{eff} from a least-squares fit of eq 2. To avoid ambiguities associated with the surface fluctuations near zero fluence, the fit is restricted to information obtained after a C_{60}^+ fluence of 1.5×10^{13} ions/cm^2. The value of S_0 is then estimated by extrapolating this curve to zero fluence. Note from eq 2 that the signal intensity must be corrected by subtracting the steady-state value (S_{ss}) prior to the semilog fit performed to obtain σ_{eff}. By combining eqs 2 and 5, it is found that

$$d = \frac{Y^{tot}}{n(S_{ss}/S_0)\sigma_{eff}} \qquad (11)$$

The value of σ_{eff} is found to be 9 nm^2, which leads to $d = 23$ nm. The value of σ_D is now determined directly from eq 5 as 5 nm^2. Considering the molecular density of trehalose, 312 molecules are damaged compared to 245 molecules being removed during one C_{60} impact. It is a fact that both numbers are of the same order of magnitude, which makes that C_{60} projectile suitable for low-damage molecular depth profiling. All of the determined parameters are summarized in Table 1, and the comparison plots of experimental and predicted results are shown in Figure 5a for pure trehalose.

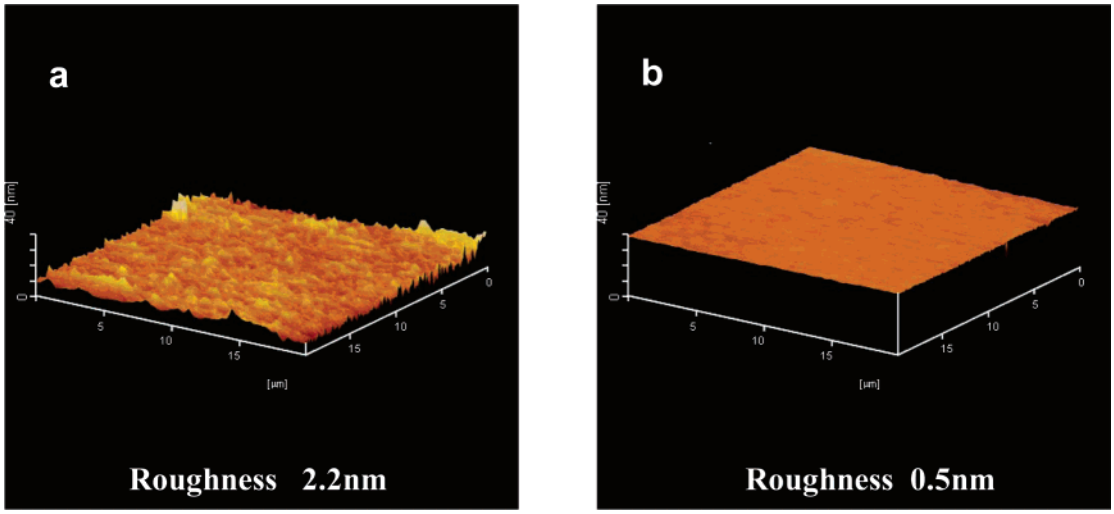

Figure 4. AFM images of (a) the original trehalose film surface before ion bombardment and (b) the surface within the eroded crater after bombardment with 20-keV C_{60}^+ (1×10^{14} cm^{-2}). The field of view is 20 μm $\times$ 20 μm. The labeled roughness corresponds to root-mean-square values determined from the statistical analysis of the entire image.

TABLE 1: Erosion Model Parameters Introduced in Section 3.1 as Evaluated from the Experimental Depth Profile Data on Pure Trehalose Films and Trehalose Film Doped with 1% GGYR or 1% KRTLRR Peptides Obtained with Au_1^+, Au_2^+, Au_3^+, and C_{60}^+ Projectiles[a]

	Tre				Tre + GGYR		Tre + KRTLRR	
					peptide	Tre	peptide	Tre
projectile	Au_1^+	Au_2^+	Au_3^+	C_{60}^+	C_{60}^+	C_{60}^+	C_{60}^+	C_{60}^+
n (nm^{-3})				2.7				
Y^{tot}	1.5	176	218 ± 12	245 ± 7	215		202	
Y_0^a	1.5	176	218 ± 12	245 ± 7	592[b]	215[b]	643[b]	202[b]
σ_{eff}(slope) (nm^2)	N/A	13 ± 4	16 ± 1	9 ± 2	16	6.6	18	6.1
σ_D (nm^2)	N/A	12 ± 5	14 ± 1	5 ± 1	3 ± 1[b]		3 ± 1[b]	
S_{ss}/S_0	N/A	0.2 ± 0.06	0.1 ± 0.03	0.5 ± 0.1	0.29	0.59	0.25	0.55
d (nm)	N/A	27 ± 2	49 ± 16	23 ± 6	17	20	17	22
interface width (nm)	N/A	27 ± 0.4	17 ± 1	7 ± 1	7.4		7.4	
c_s^{Au}	0.67	0.011	0.014	N/A	N/A		N/A	

[a] Data were averaged over three separate analyses with three different films. [b] Values calculated assuming the same damage cross section σ_D for peptide analyte and trehalose matrix molecules (see text for details).

It is interesting to consider the significance of d and σ_D. There are no molecular dynamics calculations of the ion impact event on these types of systems, but ongoing studies performed for a water-ice target for 5 keV C_{60} bombardment suggest that at 5 ps after a single C_{60}^+ impact, a crater is formed that extends to a depth of at least 7.6 nm.[2,31] This value might become slightly larger or smaller at longer times, but the calculation does provide a qualitative estimate of the order of magnitude for d, and it is within range of our measured value (see Table 1). Note also that the cross-sectional area of a C_{60} molecule is about 3.5 nm^2, a value slightly smaller than σ_D. Hence, it is likely that most of the chemical damage occurs very near the C_{60}^+ impact point. If the calculated and experimental numbers are comparable, they suggest that most of the damaged trehalose molecules are created very close to the impact crater itself.

3.3. Depth Profiles of Peptide-Doped Trehalose Films Bombarded by C_{60}^+. When the trehalose film is doped with peptide at the 1% level, similar trends are observed for both the trehalose molecular ion and the peptide molecular ion. This result is illustrated in Figure 2, parts b and c, for two different peptides with molecular weights of 451 and 829, respectively. Note that the surface fluctuation is different for each of these peptides, and that the rate and magnitude of signal decay is faster for the heavier peptide. However, a steady-state value is reached for all signals in each case. The value of Y^{tot} is dependent upon the nature of the doped peptide. This yield decreases to 215 and 202 trehalose molecular equivalents for the lighter and heavier peptide, respectively. The comparison plots of experimental and predicted results are shown in Figure 5, parts b and c, for the two peptide-doped films.

Determination of the relevant parameters from the erosion model is not straightforward for the peptide-doped films since the value of Y_0^a for the peptide is unknown. For both the trehalose matrix signal and the peptide signal, σ_{eff} is readily determined from eq 8, and d is determined from eq 11 as described above. These values are summarized in Table 1. Note that the value of d calculated from the peptide signal is very close to that determined from the trehalose signal, even though the depth profiles of both species are not identical. The damage cross section σ_D can only be determined from the matrix signal, since in this case $Y_0^a = Y^{tot}$. If we assume the same σ_D for both analyte and matrix, it is possible to calculate the theoretical sputtering yields of the peptide in the trehalose matrix environment. This assumption is reasonable since, as indicated above, σ_D should be approximately determined by the lateral dimension of the impact crater. With this assumption, the yield of peptide is about 3 times larger than the yield of sugar, implying that preferential sputtering is significantly contributing to the decline in the peptide signal reported in Figure 2b,c.

3.4. Depth Profiles of Pure Trehalose Films Bombarded by Au^+, Au_2^+, and Au_3^+ Projectiles. Because of the stability and uniformity of the sugar/peptide system, it is possible to

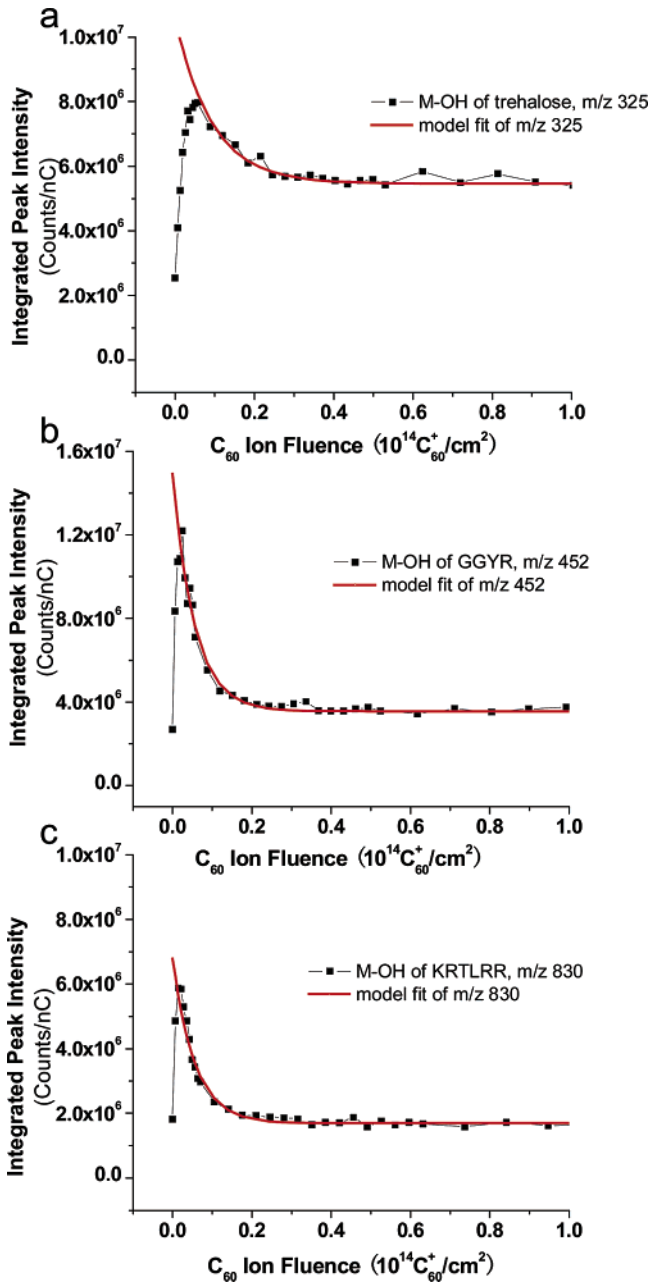

Figure 5. Comparison of experimental data as shown in Figure 2 and the prediction of the erosion model for (a) pure trehalose film (270 nm), (b) trehalose film doped with 1% GGYR (263 nm), and (c) trehalose film doped with 1% KRTLRR (273 nm). The model curves represent least-squares fits of eq 2 or eq 8 to the experimental data within the indicated fitting region.

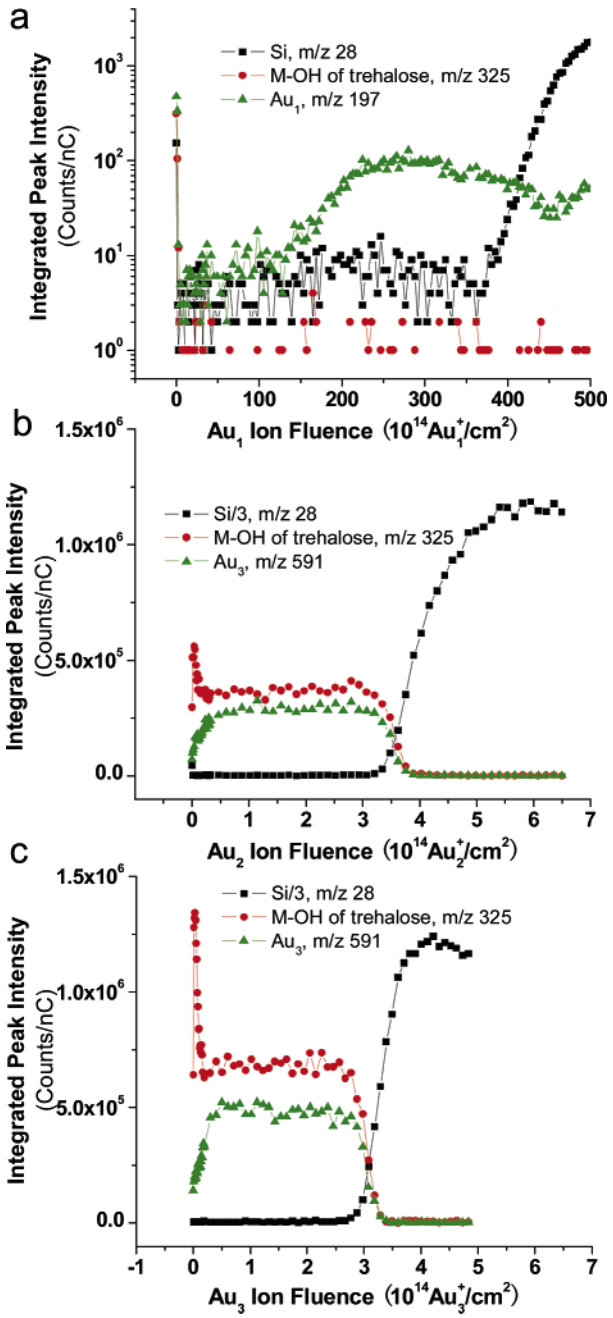

Figure 6. Secondary ion signal intensities versus accumulated fluence of (a) Au^+, (b) Au_2^+, and (c) Au_3^+ projectile ions during depth profiling of a pure trehalose film (255 nm).

evaluate the prospects for molecular depth profiling by using a variety of projectiles and to further test the suitability of our erosion model. Typical trehalose profiles with Au^+, Au_2^+, and Au_3^+ are shown in Figure 6. In this work, we report only on the behavior of the pure trehalose system without the addition of peptide analytes. As expected, no meaningful molecular depth profile can be measured with atomic Au^+ projectiles. The generic trend in the depth profiles acquired with Au_2^+ and Au_3^+ is similar to those observed of the C_{60}^+ induced depth profiles.

Before attempting a more detailed analysis, it is interesting to note that all three Au-induced depth profiles exhibit signals of both Au (*m*/*z* 197) and Au clusters (e.g., Au_3 *m*/*z* 591). These signals continue to increase with ion fluence up to about 2×10^{13} ions/cm^2, where a steady state is reached. This observation clearly indicates that there is a substantial amount of Au implantation during the bombardment process. This result is consistent with molecular dynamics simulations of 5-keV Au_3 impact onto water-ice, where all Au atoms are found to implant into the bulk of the ice sample.[31] At equilibrium, simple mass balance requires that the number of Au atoms implanted must equal the number of Au atoms sputtered. With the assumption that Y^{Au} is proportional to both Y^{tot} and the Au surface concentration, c_s^{Au}, this mass balance may be expressed as

$$Y^{Au} = m = c_s^{Au} Y^{tot} \quad (12)$$

for a projectile containing *m* constituent Au atoms. The resulting values of c_s^{Au} are displayed in Table 1. They indicate that the Au accumulation is highest for atomic projectiles due to the relatively low total sputter yield. For cluster projectiles, values of the order of 1 Au atom per 100 trehalose molecules are predicted.

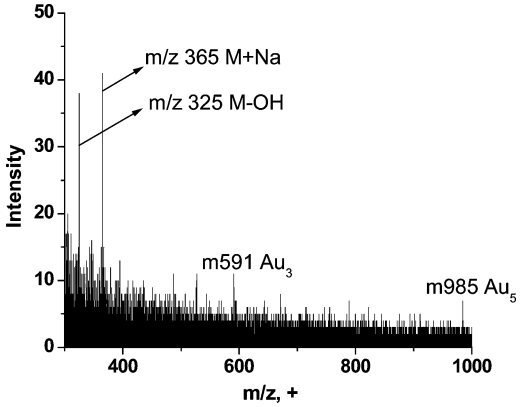

Figure 7. Time-of-flight mass spectrum taken with 25-keV Au_3^+ projectiles at a total Au_3^+ ion fluence of 1.9×10^{14} cm^{-2}.

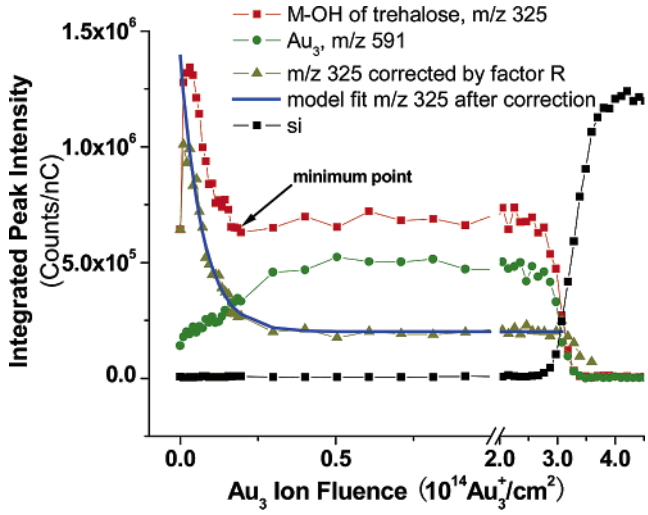

Figure 8. Comparison of the experimental depth profile of the trehalose $(M - OH)^+$ signal with and without correction for modification of the ionization probability due to Au implantation. In addition, a least-squares fit of the erosion model to the corrected $(M - OH)^+$ signal is given.

There is also evidence for the formation of gold nanoclusters during the implantation process. A mass spectrum taken at a fluence of 1.9×10^{14} Au_3^+ ions/cm^2 is shown in Figure 7, where Au_3^+ and Au_5^+ secondary ion emission is readily seen. This observation requires the simultaneous emission of many Au atoms in a single projectile impact event. Since the overall concentration should be on the order of 1% as shown in Table 1, it is likely that these clusters arise from Au atoms that were near each other in the solid, indicating that they were not randomly distributed through the surface region.

The Au implantation also exerts a subtle influence on the Au_2^+ and Au_3^+ depth profiles of trehalose films. From the data shown in Figure 8, a shallow minimum of trehalose molecular ion signal intensity is seen at a fluence of 2×10^{13} ions/cm^2. The increase in signal intensity at higher fluences follows closely the increase in the amount of implanted Au. Since it is known that evaporation of Au onto the analyzed surface enhances the molecular secondary ion yield in static SIMS experiments,[32,33] we speculate that this increase in signal is associated with the formation of the altered matrix. More detailed analysis becomes problematic, since this effect perturbs the shape of the depth profile in a region critical for fitting with use of the erosion model. It is possible to make some approximations to account for the enhanced ionization effect induced by Au implantation. We define a factor $R = S_0^{Au}/S^{Au}$, where S^{Au} is the Au_3^+ secondary ion signal intensity at any fluence point, while S_0^{Au} is the initial Au_3^+ secondary ion signal intensity at zero fluence. The Au_3^+ signal is used here instead of Au^+ to monitor the gold concentration in the altered layer, since there are isobaric interferences at mass 197 that prevent simple use of this peak. Normally, S_0^{Au} is found to be very close to zero and constitutes a background signal. Assuming the ionization probability to be directly proportional to the Au concentration in the altered layer, the signal intensity of the molecular ion at *m*/*z* 325 is then corrected by the factor *R*, and the erosion model is then applied to fit the corrected profile as shown in Figure 8. After this correction, the altered layer thickness is found to be on the order of 20 nm. Other relevant values are also listed in Table 1.

4. Conclusions

From the studies reported here, we find that successful molecular depth profiles may be acquired on trehalose films with use of all of the employed projectiles except for Au^+. Profiles acquired with the C_{60}^+ projectile are somewhat better than those obtained with the Au_m^+ cluster ions, since C_{60}^+ produces the highest sputtering yield and the lowest value of *d*. It is also interesting that the ion yield for the *m*/*z* 325 trehalose ion observed under steady-state conditions is about an order of magnitude larger for C_{60}^+ than that for the Au_m^+ projectiles as seen from the scale of the intensity axes shown in Figures 2a, Figure 6b, and Figure 6c. Although this observation is not relevant for the application of the erosion model to the depth profile, it does suggest that there may be some fundamental differences in the ionization mechanism associated with both classes of projectiles.

Finally, we note that even though the proposed model is highly simplified, it does provide a good fit to the experimental data by using fitting parameters that have reasonable physical significance. Computer simulations on Ag{111} have shown that the sputtering yield increases faster (from 49 to 482) than the crater depth (from 1.5 to 2.1 nm) as the kinetic energy is increased from 5 to 20 keV.[19] The prediction that high sputtering yield and low altered layer thickness will lead to the lowest chemical damage buildup suggests that even better depth profiles may be acquired by using larger or higher kinetic energy projectiles.

Acknowledgment. The authors would like to acknowledge partial financial support provided by the NIH and the NSF.

References and Notes

(1) Gillen, G.; Roberson, S. *Rapid Commun. Mass Spectrom.* **1998**, *12*, 1303.
(2) Cheng, J.; Winograd, N. *Anal. Chem.* **2005**, *77*, 3651.
(3) Wucher, A.; Sun, S.; Szakal, C.; Winograd, N. *Anal. Chem.* **2004**, *76*, 7234.
(4) Sostarecz, A. G.; McQuaw, C. M.; Wucher, A.; Winograd, N. *Anal. Chem.* **2004**, *76*, 6651.
(5) Wagner, M. S. *Anal. Chem.* **2005**, *77*, 911.
(6) Mahoney, C. M.; Roberson, S.; Gillen, G. *Appl. Surf. Sci.* **2004**, *231*−*232*, 174.
(7) Winograd, N. *Anal. Chem.* **2005**, *77*, 142A.
(8) Wagner, M. S.; Gillen, G. *Appl. Surf. Sci.* **2004**, *231*−*232*, 169.
(9) Mahoney, C. M.; Roberson, S. V.; Gillen, G. *Anal. Chem.* **2004**, *76*, 3199.
(10) Davies, N.; Weibel, D. E.; Blenkinsopp, P.; Lockyer, N.; Hill, R.; Vickerman, J. C. *Appl. Surf. Sci.* **2003**, *203*, 223.
(11) Touboul, D.; Kollmer, F.; Niehuis, E.; Brunelle, A.; Laprevote, O. *J. Am. Soc. Mass Spectrom.* **2005**, *16*, 1608.
(12) Weibel, D. E.; Lockyer, N.; Vickerman, J. C. *Appl. Surf. Sci.* **2004**, *231*−*232*, 146.
(13) Crowe, J. H.; Crowe, L. M.; Chapman, D. *Science* (*Washington, D.C.*) **1984**, *223*, 701.
(14) Westh, P.; Ramlov, H. *J. Exp. Zool.* **1991**, *258*, 303.

(15) Crowe, J. H.; Crowe, L. M. *Nat. Biotechnol.* **2000**, *18*, 145.
(16) Xia, N.; Shumaker-Parry, J. S.; Zareie, M. H.; Campbell, C. T.; Castner, D. G. *Langmuir* **2004**, *20*, 3710.
(17) Xia, N.; May, C. J.; McArthur, S. L.; Castner, D. G. *Langmuir* **2002**, *18*, 4090.
(18) Winograd, N. *Mat. Fys. Medd. K. Dan. Vidensk. Selsk.* **1994**, *43*, 223.
(19) Postawa, Z.; Czerwinski, B.; Szewczyk, M.; Smiley, E. J.; Winograd, N.; Garrison, B. J. *J. Phys. Chem. B* **2004**, *108*, 7831.
(20) Postawa, Z.; Czerwinski, B.; Szewczyk, M.; Smiley, E. J.; Winograd, N.; Garrison, B. J. *Anal. Chem.* **2003**, *75*, 4402.
(21) Webb, R.; Kerford, M.; Way, A.; Wilson, I. *Nucl. Instrum. Methods Phys. Res., Sect. B* **1999**, *153*, 284.
(22) Aoki, T.; Seki, T.; Matsuo, J.; Insepov, Z.; Yamada, I. *Mater. Chem. Phys.* **1998**, *54*, 139.
(23) Insepov, Z.; Yamada, I.; Sosnowski, M. *Mater. Chem. Phys.* **1998**, *54*, 234.
(24) Takeuchi, D.; Seki, T.; Aoki, T.; Matsuo, J.; Yamada, I. *Mater. Chem. Phys.* **1998**, *54*, 76.
(25) Postawa, Z.; Ludwig, K.; Piaskowy, J.; Krantzman, K.; Winograd, N.; Garrison, B. J. *Nucl. Instrum. Methods Phys. Res., Sect. B* **2003**, *202*, 168.
(26) Wojciechowski, I. A.; Sun, S.; Szakal, C.; Winograd, N.; Garrison, B. J. *J. Phys. Chem. A* **2004**, *108*, 2993.
(27) Gillen, G.; Simons, D. S.; Williams, P. *Anal. Chem.* **1990**, *62*, 2122.
(28) Wagner, M. S. *Anal. Chem.* **2004**, *76*, 1264.
(29) Braun, R. M.; Blenkinsopp, P.; Mullock, S. J.; Corlett, C.; Willey, K. F.; Vickerman, J. C.; Winograd, N. *Rapid Commun. Mass Spectrom.* **1998**, *12*, 1246.
(30) Weibel, D.; Wong, S.; Lockyer, N.; Blenkinsopp, P.; Hill, R.; Vickerman, J. C. *Anal. Chem.* **2003**, *75*, 1754.
(31) Russo, M. F.; Wojciechowski, I. A.; Garrison, B. J. *Appl. Surf. Sci.* In press.
(32) Delcorte, A.; Medard, N.; Bertrand, P. *Anal. Chem.* **2002**, *74*, 4955.
(33) Marcus, A. J.; Winograd, N. *Anal. Chem.* **2005**, *78*, 141.